Delft University of Technology

Analysis of Nonisothermal Rarefied Gas Flow in Diverging Microchannels for Low-Pressure Microresistojets

Cordeiro Guerrieri, Daduí; Cervone, Angelo; Gill, Eberhard

Important note
To cite this publication, please use the final published version (if applicable).
Please check the document version above.

Analysis of Non-Isothermal Rarefied Gas Flow in Diverging Microchannels for Low Pressure Micro-Resistojets

Daduí C. Guerrieri
Space System Engineering
Faculty of Aerospace Engineering
Delft University of Technology
Delft, The Netherlands
Email: D.CordeiroGuerrieri@tudelft.nl

Angelo Cervone
Space System Engineering
Faculty of Aerospace Engineering
Delft University of Technology
Delft, The Netherlands
Email: A.Cervone@tudelft.nl

Eberhard Gill
Chair of Space System Engineering
Faculty of Aerospace Engineering
Delft University of Technology
Delft, The Netherlands
Email: E.K.A.Gill@tudelft.nl

Heat transfer and fluid flow through different microchannel geometries in the transitional regime (rarefied flow) are analysed by means of Direct Simulation Monte Carlo simulations. Four types of three-dimensional microchannels, intended to be used as expansion slots in micro-resistojet concepts, are investigated using Nitrogen as working fluid. The main purpose is to understand the impact of the channel geometry on the exit velocity and the transmission coefficient, parameters which are well known to affect directly the thruster performance. Although this analysis can be applied in principle to several possible microfluidics scenarios, particular focus is given to its application in the field of space propulsion for micro-, nano- and pico-satellites, for which the requirements ask for low thrust levels from some μN to a few mN and moderate specific impulse, as well as a low power consumption in the order of a few W. Analysis shows that the thrust produced by one single microchannel can be increased by about 480% with a careful selection of the channel geometry, decreasing at the same time the specific impulse by just 5%, with a power consumption decrease of more than 66.7%.

1 Introduction

The past decade has seen a massive growth in the number of small satellites lauched into Earth orbit. This has led, in turn, to a significant increment of the research activities on the miniaturization of satellite subsystems and components. However, in order to reduce mass and cost, typically nano-satellites (i.e., satellites with a mass between 1 and 10 kg) are still designed without any propulsion capabilities, and only very recently micro-propulsion systems have started to be developed and demonstrated in flight. Thus, their mission lifetime and performance are severely limited [1, 2].

Nano-satellites are typically used in Low-Earth Orbit (LEO), where some specific missions might require a capable propulsion system to enable, for instance, formation flying, orbit change and/or station keeping of constellations. These propulsion systems need to be extremely miniaturized and highly integrated; they shall usually provide thrust levels in the order of some μN up to a few mN, with a limited power consumption [3, 4]. In addition, there is currently a societal urge to use "green" space systems, that shall be free of components or materials publicly recognized as toxic or potentially hazardous for the environment. Finally, current nano-satellite regulations demand for propellants that shall be non-corrosive, non-flammable and non-toxic [5].

A particular propulsion concept based on rarefied gas dynamics, denoted as Free Molecule Micro-Resistojet (FMMR), has started to be proposed in the late 90's as an alternative to meet the specific requirements and constraints imposed by nano-satellites [6, 7]. Ketsdever et al. [6] presented several advantages of this concept when compared with more traditional micro-thrusters, such as reduced tank pressure, avoidance nozzle plugging, ease and flexibility of construction and reduced valve actuation. An important part of the system is the thrust chamber, or heater chip, usually characterized by a flat plate geometry with expansion slots or microchannels in which molecules are heated, accelerated and expelled into space [8]. As an example, the geometry proposed by Ketsdever et al. [9] is a 19.2 x 19.2 mm square,

500 μm thick, manufactured on a double-sided silicon wafer. It contains 44 expansion slots with dimensions of 100 μm wide by 5.375 mm long. The performance of this heater chip was numerically simulated by a Direct Simulation Monte Carlo (DSMC) code, using Nitrogen as molecular species, and successively compared to experimental data, showing a good agreement with a difference of no more than 2% [10].

Rarefied gas dynamics is relevant to a large number of different applications such as vacuum technology and space dynamics, all characterized by a low pressure environment [11, 12]. Nowadays, it is also becoming more and more relevant to the design and study of microfluidic devices intended for several applications. The first microsystem device for microfluidic application, an integrated cooling system for electronic circuits with a power density of 790 W/cm^2, dates back to the 80's [13]. This system allowed small electronic devices, producing high temperature when in operation, to keep working at better efficiency. The main advantage in using microchannels is their extremely high surface area to volume ratio when compared with large channels. However, rarefaction, compressibility, viscous heating and thermal creep are important possible drawbacks that are well known to affect the flow dynamics of MEMS [14].

Rarefied gas flows can be classified in three different regimes: the continuum regime with slip flow, the transition flow, and the free molecular flow. The Knudsen number defines the degree of gas rarefaction. It depends on the average distance travelled by the molecules between collisions, known as the *mean free path*, λ, and the *characteristic dimension*, L. The Knudsen number is expressed as:

$$Kn = \frac{\lambda}{L_0} \qquad (1)$$

Its value defines if the flow shall be classified as slip flow, for Knudsen number in the range from 0.01 to 0.1, transition flow, from 0.1 to 10, or free molecular flow, for Knudsen numbers higher than 10 [14, 15].

The Navier-Stokes equations describe the fluid dynamics in the continuum flow regime, but they can not predict the solution of the transition flow regime; in this case, the Boltzmann equation is applied [14, 15]. The Boltzmann equation is not solved directly by DSMC, since it analyses the motion of the particles or molecules in a small volume by means of probabilistic physical simulations [16]. In DSMC simulations, the particles or molecules are represented by a sample and not by their actual total number, in order to keep the simulation at an acceptable level in terms of computational cost. However, under adequate conditions, the probabilistic results still gives a good approximation of the solution [15].

The transition flow regime is usually the nominal operational condition of FMMR devices due to the low operational pressure of the system, and the DSMC method is a consolidated tool to study the fluid dynamic and thermal properties in this regime. Several previous research activities have studied fluid dynamics in microchannels using the DSMC, showing how the aspect ratio, temperature and Knudsen number influence the gas behaviour [17–20]. In some cases, the pressure drop, temperature and velocity through the channel are also analysed. Even though some researchers have also been using the DSMC method to analyse the micronozzle performance for the transition between the slip flow regime and the transition flow regime [21–24], there is still a lack of micronozzle performance analysis in case at the boundary between the transition flow and the molecular flow regimes (Knudsen number larger than 0.1).

The aspect ratio of the expansion channel, defined as thickness to diameter ratio, is an important parameter that has to be considered in this concept. Normally, the mass flow rate decreases with increasing aspect ratio. One disadvantage in decreasing the aspect ratio is that the heat transfer also decreases. The portion of mass flow rate that goes through a channel is defined by the "transmission coefficient", α, which is also known as conductance [11] or dimensionless mass flow rate [20, 25]. It is the actual mass flow rate to the mass flow rate in free molecular limit ratio, which is expressed in the form of $\alpha = \dot{m}/\dot{m}_{fm}$, meaning that for an infinitely thin channel, the transmission coefficient is equal to 1. For a cylindrical channel with an aspect ratio of 5, a typical value of the transmission coefficient is 0.19 [11,20].

From the thruster point of view, the thrust $\Im$ increases with the mass flow rate $\dot{m}$ and the flow exit velocity u_e, see equation (2), whereas the specific impulse I_{sp} tends to slightly decrease with the mass flow rate, equation (3). When the heat transfer from the channel walls to the fluid increases, the exit velocity and the exit pressure P_e increase, and, consequently, the thrust and specific impulse increase too.

$$\Im = \dot{m}u_e + (P_e - P_a)A_e \qquad (2)$$

$$I_{sp} = \frac{\Im}{\dot{m}g_0} \qquad (3)$$

where in equations 2 and 3, P_a is the ambient pressure (zero in vacuum), A_e is the thruster exit area, and g_o is the Earth gravitational acceleration at sea level.

This article presents a sensitivity analysis of the thruster performance as function of the microchannel geometry. A microchannel aspect ratio of 4.4 is used as a baseline and different divergent microchannel geometries are simulated. The channel geometry influences the transmission coefficient and the heat transfer performance that, in turn, directly influence the thruster performance. The purpose is to propose a design in which better thrust level can be achieved, without any substantial drop in the specific impulse and, possibly, with a reduction of the specific energy.

2 Numerical Modelling

The 3-D DSMC code *dsmcFoam*, in particular the open source C++ CFD toolbox *OpenFOAM*, has been used to analyse the flow dynamics and thermal properties of the system.

As in all DSMC tools, the motion of particles/molecules in a small cell volume (Δx_{cell}) is analyzed. In each cell, a set of representative collisions is processed at each time step (Δt_{step}). The DSMC does not use the actual number of particles due to the high simulation cost required, even though the sample of particles use in the simulations represent well the solution. These parameters play an important role on the accuracy of the simulation and they are estimated according to [15] as:

$$\Delta x_{cell} \leq \frac{\lambda}{3} \tag{4}$$

$$\Delta t_{step} = \frac{\xi \lambda}{\bar{c}} \tag{5}$$

where ξ is the fraction of mean free time (the mean time between collisions) at the mean stream conditions, and $\bar{c}$ is the mean thermal speed. According to the equations above the mesh size has to be less than 12 μm and the time step has to be close to 2×10^{-7} s. Additionally, the typical value of the actual- to simulated-particle ratio S per cell is taken in the range from 10^{14} to 10^{18} for a three-dimensional computation [26]. On the other hand, values of S close to 1 are typically used to simulate completely free molecular flows. However, in the cases studied in this paper, both the transitional and the free molecular regimes are present, and for this reason an intermediate value has been chosen for S. This means that the flow regions under the free molecular regime, which are less interesting for the scopes of this study, have been simulated less accurately due to the relatively low number of particles considered. Taking these constraints into account, an affordable value of S (in terms of computational cost) was defined. Table 1 shows a summary of the main simulation parameters, set in agreement with the indications provided by literature and common practice [15, 26, 27].

A sketch of the baseline modelling (case 1) can be seen in Figure 1. It is divided in three sections: a portion of the plenum, the microchannel and a portion of the outer space. The main purpose of these simulations is to understand and characterize the gas behaviour into the channel, with portions of the plenum and the outer space simulated in order to better understand how the external and boundary conditions influence the fluid dynamics into the channel. The reference frame is placed with its origin at the channel entrance (x=0), with the channel exit at x=L=500 μm. The microchannel is designed with a circular cross-sectional area of 10,000 μm^2. The inlet boundary condition is represented by a blue line, and corresponds to a plenum or reservoir under stagnation conditions at a temperature of 300 K and a pressure of 50, 150 or 300 Pa depending on the simulated case. Vacuum conditions are imposed at the outlet boundary that is represented by a black line and corresponds to the outer space. The channel wall boundary condition (red line) was considered at a fixed constant temperature, namely 300, 573, 700 or 900 K depending on the simulated case. Additionally,

Table 1. Simulation setting according to [15, 27]

Element	Model/Value
Gas interaction	Variable Hard Sphere
Energy exchange	Larsen-Borgnakke
Gas-Surface interaction	Diffuse
Molecular Species	N_2 (nitrogen)
Rotational degree of freedom	2
m	46.5×10^{-27} kg
d_{ref}	4.17×10^{-10} m
ξ	0.1
ω	0.74
Δx_{cell}	$\leq 5\mu m$
Δt_{step}	2×10^{-7}s
S	10^4

Table 2. Variable parameters for the different cases analysed

Cases	P_0 [Pa]	T_w [K]	β [°]	Kn_{in}	Π
	50	300 - 900	0	1.3	13 - 17
1	150	300 - 900	0	0.4	14 - 17
	300	300 - 900	0	0.3	14 - 17
2	150	573	0 - 40	0.5	15 - 262
3	150	573	0 - 40	0.5	15 - 480
4	150	573	0 - 40	0.5	15 - 35

the green dashed line represents a symmetric plane boundary condition, applied to simplify the modelling and reduce the simulation time. The variable parameters used for different cases are summarized in Table 2.

Moreover, three additional configurations with a (partially) divergent microchannel were simulated. Figure 2 shows the four cases which were analysed, namely: case 1 (Baseline microchannel), case 2 (Entirely divergent microchannel), case 3 (Second-half divergent microchannel), and case 4 (First-half divergent microchannel). The same inlet cross-sectional area has been used for all the cases. The angle of the divergent part, β, has been varied from 0 to 40° for each case. The same boundary conditions and parameters as in the baseline have been used, but only one value of the plenum pressure (150 Pa) and wall temperature (573 K) has been considered for cases 2, 3 and 4. This choice is motivated and discussed in the next section, together with the results achieved.
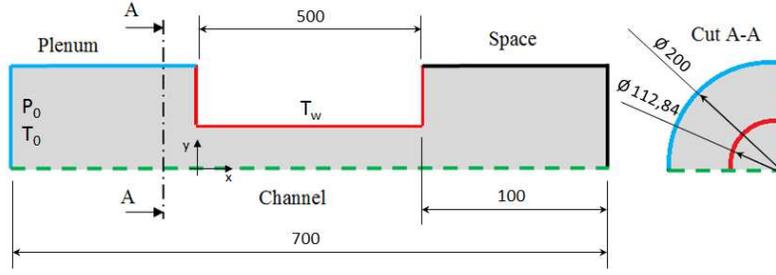
Fig. 1. Scheme of the baseline microchannel modelling (case 1, dimensions in μm). The plenum boundary condition is represented by a blue line, the channel wall by a red line, the space by a black line and the green dashed line represents the symmetric plane boundary conditions.
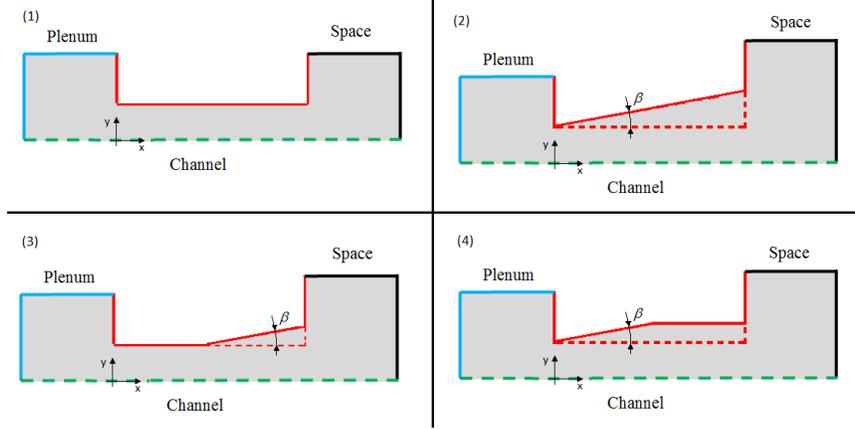
Fig. 2. Scheme of the four configurations analysed. (1) Baseline microchannel, (2) Entirely divergent microchannel, (3) Second-half divergent microchannel, and (4) First-half divergent microchannel.

3 Results and Discussion
3.1 DSMC validation

To validate the numerical parameters used for the simulations, a plenum pressure of 50 Pa and a wall temperature of 300 K have been used. The Knudsen number in the channel varies between 1.1, at the channel entrance, and 14.2, at the channel exit. Besides the baseline cell size of 5 μm, two other values were tested: 2.5 μm and 10 μm. Table 3 shows the mean exit velocity and the mean exit pressure for different cell size values. The exit pressure does not show significant variations, but for the exit velocity a difference of 1.3% (in the worst case) in relation to the baseline parameter is present. For the time step, besides the baseline of 2×10^{-7} s, two other values were tested: 1×10^{-7} s and 5×10^{-7} s. Table 3 shows the results in terms of the mean exit velocity and the mean exit pressure. The exit pressure also in this case does not show significant changes, but the exit velocity presents a difference of 1.9% in the worst case. Another numerical parameter that has been validated is the particles-per-cell value. Besides the actual- to simulated-particle ratio S of 10^4, two other values were tested: 10^3 and 10^5, see Table 3. The exit pressure also does not show significant changes and the exit velocity presents a difference of 1.3% in the worst case. In conclusion, the uncertainty is expected to be not bigger than 2.6%.

An additional validation has been carried out by comparing the pressure variation along the channel centerline from the current numerical code to an analytical expression given in [14]:

$$
\tilde{P}^2 - 1 + 2(6+\bar{\alpha})\frac{2-\sigma_v}{\sigma_v}Kn_o(\tilde{P}-1)+
$$
$$
2(6b+\bar{\alpha})\frac{2-\sigma_v}{\sigma_v}Kn_o^2 log_e\left(\frac{\tilde{P}-bKn_o}{1-bKn_o}\right) = B\left(1-\frac{x}{L}\right),
$$
(6)

Table 3. Comparison of numerical results obtained with different parameters.

Parameters		u_e [m/s]	P_e [Pa]	Difference [%]
	2.5 μm	297	2.8	1.3
Δx_{cell}	5 μm	301	2.8	—
	10 μm	299	2.8	0.7
	1×10^{-7} s	302	2.8	0.1
Δt_{step}	2×10^{-7} s	302	2.8	—
	5×10^{-7} s	296	2.7	1.9
	10^3	301	2.8	0.3
S	10^4	302	2.8	—
	10^5	298	2.8	1.3

where $\tilde{P}$ is the ratio of local pressure to outlet pressure, Kn_o is the outlet Knudsen number, σ_v is the thermal accommodation (set equal to 1), B is a constant such that $\tilde{P} = P(x = 0)/P_o$, and b and $\bar{\alpha}$ are constants too. The comparison is presented in Figure 3, which shows very good matching with the findings of [14], where it is indicated that at higher Knudsen numbers and, thus, under free molecular flow conditions, the pressure distribution along the channel centerline is much closer to what would be obtained by assuming a linear pressure drop. Equation 6 gives however still sufficiently accurate results, with a maximum difference of 3.0% for a plenum pressure of 50 Pa, 2.7% for a plenum pressure of 150 Pa, and 2.9% for a plenum pressure of 300 Pa. A wall temperature of 300 K was used for this comparison.
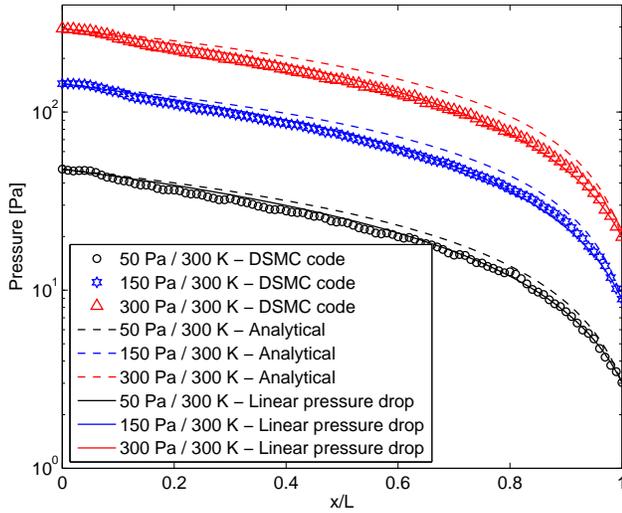
Fig. 3. Pressure along the channel centerline: comparison of the current DSMC code with the analytical solution from [14]

3.2 Case 1. Baseline microchannel analysis

In Figure 4, the normalized pressure along the channel is shown for different plenum pressures and wall temperatures. The pressure slightly raises in the first part of the channel, followed by a gradual decrease very close to a linear function, where the linear coefficient depends mainly on the plenum pressure. Furthermore, when the wall temperature is the same as the plenum temperature (in this study 300 K), the entrance pressure is less than the plenum pressure. On the other hand, when the wall temperature exceeds the plenum temperature, the entrance pressure is larger. The normalized mean pressure at the channel inlet mainly depends on the channel wall temperature, although it obviously converges to the same value at the channel outlet.

Due to the random direction of particles and the high number of collisions in the channel entrance area, the heat transfer from wall to particles is more effective in the first 30% of the channel length, after which the mean gas temperature is constant and close to the wall temperature, see Figure 5. The mean gas temperature decreases a bit in the
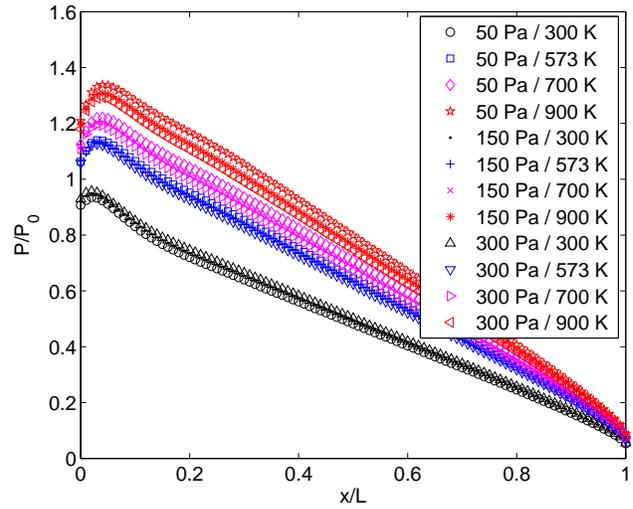
Fig. 4. Mean pressure along the channel (normalized) for the baseline microchannel (case 1), for different plenum pressures and wall channel temperatures.

last 20% of the channel due to the low outer space temperature. The complete temperature field is shown in Figure 6-(a) for plenum pressure of 150 Pa and wall temperature of 573 K.
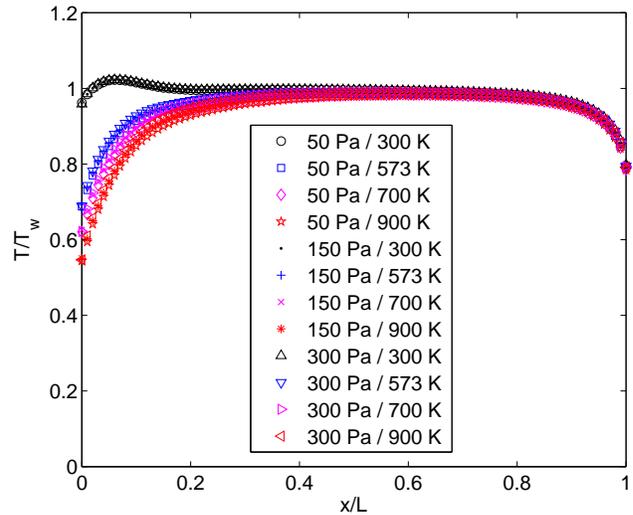
Fig. 5. Mean temperature along the channel (normalized) for the baseline microchannel (case 1), for different plenum pressures and wall channel temperatures.

Since there is no change in the cross-sectional area along the baseline channel, the Mach number along the channel presents a similar value for the different cases studied independently on the Knudsen number, plenum pressure and channel wall temperature. The Mach number converges to sonic velocity at the channel outlet, see Figure 6-(b). The Knudsen number depends mainly on the plenum pressure and channel wall temperature: when the plenum pressure increases the Knudsen number tends to decrease, and when the
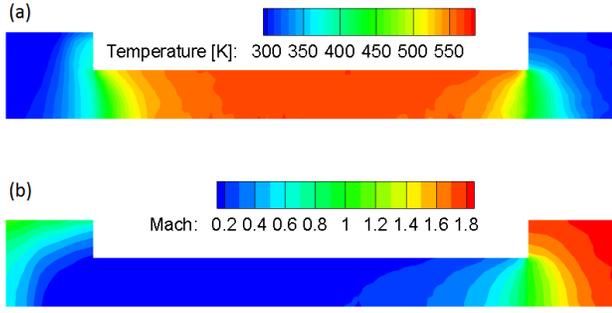
Fig. 6. Temperature (a) and Mach number (b) maps for a plenum pressure of 150 Pa and channel wall temperature of 573 K, for the baseline microchannel (case 1).

wall temperature increases the Knudsen number tends to increase, see Table 4. For plenum pressure of 50 Pa the flow regime turns into a free molecular flow in the last part of the channel.

Table 4. Knudsen number at the channel inlet and outlet, baseline microchannel (case 1).

P_0[Pa]	T_w[K]	300	573	700	900
50		1.1	1.3	1.4	1.5
150	Kn_{in}	0.4	0.4	0.5	0.5
300		0.2	0.2	0.2	0.3
50		14.2	20.1	22.3	25.4
150	Kn_{out}	4.6	6.9	7.7	8.9
300		2.3	3.6	4.0	4.7
50		17.0	14.9	14.4	13.7
150	Π	16.7	15.2	14.6	14.1
300		16.8	15.6	15.2	14.6

The molecules are accelerated in the microchannel mainly due to collisions with the hot channel walls, and the exit velocity increases from 293 to 503 m/s when the channel wall temperature increases from 300 to 900 K, respectively. Table 5 shows the transmission coefficient and exit velocity for different channel wall temperatures and plenum pressures. Varying from 17 to 19 %, the transmission coefficient changes are not significant, although the increase in exit velocity is significant. Therefore, one initial step to improve the transmission coefficient was expected to be by a divergent channel, helping the particles to be expelled more effectively. The results obtained by using different types of divergent geometries are presented in the next subsections.

3.3 Case 2. Entirely divergent microchannel analysis

The main effect of the divergent channel is to alleviate the problems caused by the high entrance pressure, so that

Table 5. Transmission coefficient and Exit Velocity, baseline microchannel (case 1).

P_0[Pa]	50	150	300	50	150	300
T_w[K]	Transmission Coefficient			Exit Velocity [m/s]		
300	0.189	0.189	0.190	292	283	299
573	0.187	0.183	0.179	401	403	411
700	0.186	0.181	0.176	442	444	453
900	0.186	0.180	0.174	499	503	514

the passage of molecules throughout the channel is facilitated, as seen in Figure 7. The entrance pressure goes significantly down with increasing angle of the divergent part. This reduction is up to about 75% with respect to the baseline (i.e., no divergence angle), for a divergence angle of 40 degrees. In addition, the pressure drops dramatically through the microchannel, with most of this drop moved towards the channel inlet when the divergence angle increases. The channel exit pressure also decreases with increasing divergence angle.
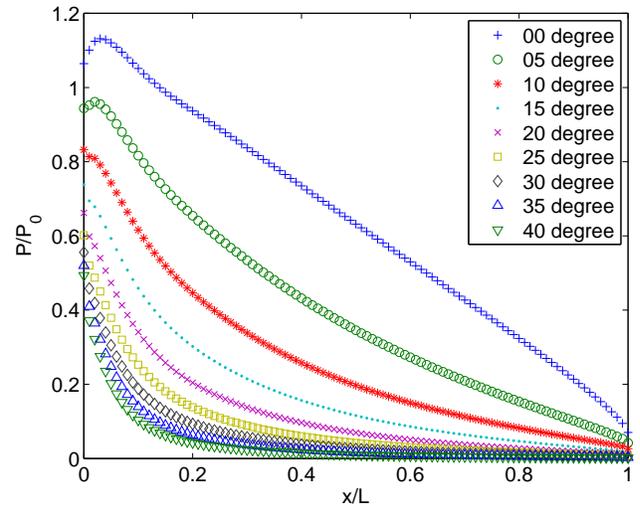
Fig. 7. Mean pressure along the channel, entirely divergent microchannel (case 2), for different divergent angles at a plenum pressure of 150 Pa and wall temperature of 573 K.

Although on one hand the desired reduced entrance pressure effect is achieved, on the other hand the heat transfer becomes less effective than the baseline and the maximum temperature is less close to the channel wall temperature, as seen in Figure 8. When the divergent angle increases, the number of collisions decreases (in particular the particle-surface ones) and the heat transfer becomes less efficient. The complete temperature field for the case of divergent angle equal to 25 degrees can be seen in Figure 9-(a).

The gas temperature decrease at higher divergent angles implies that the molecules are accelerated less efficiently by the hot channel walls through collisions. However, when the

Fig. 8. Mean temperature along the channel, entire divergent microchannel (case 2), for different divergent angles at a plenum pressure of 150 Pa and wall temperature of 573 K.

Table 6. Knudsen number at the channel inlet and outlet, entirely divergent microchannel (case 2), for different divergent angles at a plenum pressure of 150 Pa and wall temperature of 573 K.

$\beta[°]$	05	10	15	20
Kn_{in}	0.5	0.5	0.6	0.6
Kn_{out}	10.9	16.2	23.3	32.6
$\prod$	22.5	31.7	43.9	61.2
$\beta[°]$	25	30	35	40
Kn_{in}	0.6	0.6	0.6	0.7
Kn_{out}	44.7	60.1	79.9	105.2
$\prod$	86.1	122.75	177.8	261.6

The exit velocity increases gradually from 402.5 to 461.5 m/s when the divergent angle raises from 0 to 30 degrees, respectively. For values higher than 30 degrees the exit velocity slightly decreases, Figure 10. Although the exit velocity only shows a relatively moderate change with respect to the baseline, the transmission coefficient increases significantly when the divergent angle increases, going from 18 to 93% for a divergent angle values from 0 to 40 degrees. This represents an increase of about 80% in mass flow rate effectively expelled by the channel.

(a)

Temperature [K]: 300 350 400 450 500 550

(b)

Mach: 0.2 0.4 0.6 0.8 1 1.2 1.4 1.6 1.8

Fig. 9. Temperature (a) and Mach number (b) maps for the entirely divergent microchannel (case 2), for a divergent angle of 25 degrees, plenum pressure of 150 Pa and wall temperature of 573 K.
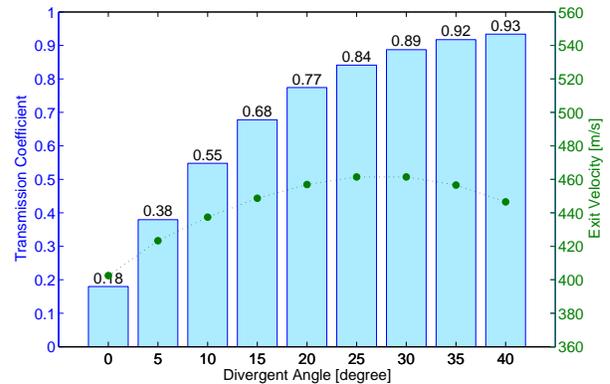
Fig. 10. Transmission coefficient and exit velocity for different divergent angles at a plenum pressure of 150 Pa and wall temperature of 573 K, entirely divergent microchannel (case 2).

divergent angle increases, the acceleration due to thermal expansion, which characterizes the more conventional propulsion concepts, increases. For this reason the Mach number increases, and the flow becomes supersonic at the channel for divergent angles higher than 10 degrees. Figure 9-(b) shows the increasing Mach number throughout the channel at a divergent angle of 25 degrees. The increasing divergent angle makes the Knudsen number rise dramatically through the channel as it can be seen in Table 6, meaning that flow goes in the free molecular regime before being expelled at the channel exit.

3.4 Case 3. Second-half divergent microchannel analysis

As it has been shown in the previous subsection, the entirely divergent angle geometry (case 2) shows an important increase in mass flow rate, but a less effective heat transfer is obtained. In case 3, the idea is to increase the heat transfer effectiveness in the first half of the microchannel (constant area) and improve the thermal expansion of the flow and, thus, the transmission coefficient in the second half (diver-

gent). Figure 11 shows that the entrance pressure is slightly reduced when the divergent angle increases up to 25 degrees, while for angles higher than 25 degrees it does not change significantly. Generally speaking, the pressure through the channel decreases significantly with the divergent angle, as well as the exit pressure.
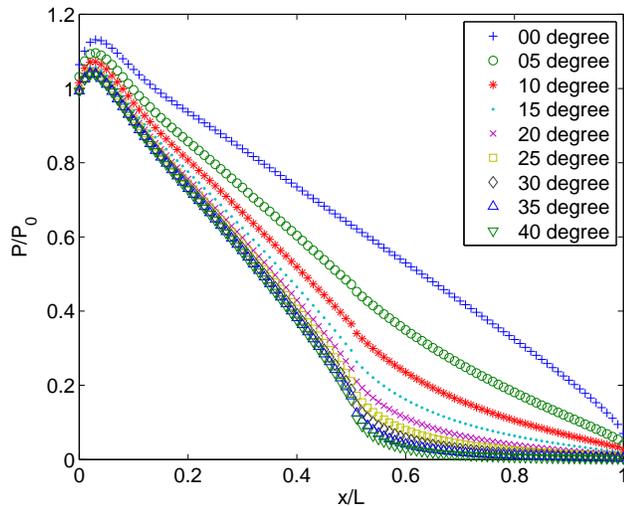
Fig. 11.   Mean pressure along the channel, second-half divergent microchannel (case 3), for different divergent angles at a plenum pressure of 150 Pa and wall temperature of 573 K.

The heat transfer does not show significant changes with increasing divergent angle, because the gas is mainly heated in the first half of the channel and, when the molecules enter in the divergent part, they are already aligned and the number of collisions with the walls are insignificant. Due to this, the gas temperature in the second half of the channel decreases significantly when the divergent angle increases, see Figure 12. The complete temperature field for a divergent angle of 25 degrees can be seen in Figure 13-(a).

Differently to the previous geometry (case 2), the Mach number presents a significant increase only in the second half of the microchannel, but still converges to similar supersonic values at the channel exit, compare Figures 9-(b) and 13-(b). The Knudsen number at channel outlet for this configuration is as high as in case 2, and the flow also goes in the free molecular regime before the channel exit, see Table 7.

A significant difference can be noticed in the exit velocity and the transmission coefficient, by comparing Figures 10 and 14. The exit velocity increases with respect to case 2 (for instance 496.1 m/s instead of 461.5 m/s, for same divergent angle of 30 degrees). The highest exit velocity (500.1 m/s) is achieved for a divergent angle of 35 degrees and there is a slight decrease for divergent angles larger than 35 degrees. The transmission coefficient presents an increase with respect to the baseline (case 1) but is significantly lower with respect to the entirely divergent angle (case 2). This happens because the mass flow rate is limited by the presence of the first constant-area of the microchannel independently
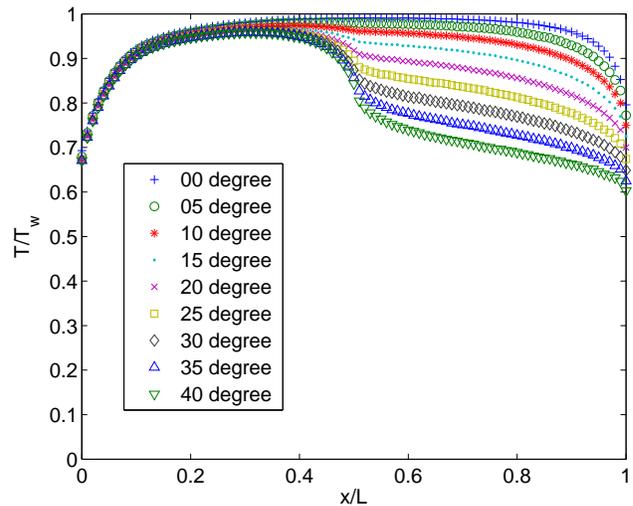
Fig. 12.   Mean temperature along the channel, second-half divergent microchannel (case 3), for different divergent angles at a plenum pressure of 150 Pa and wall temperature of 573 K.
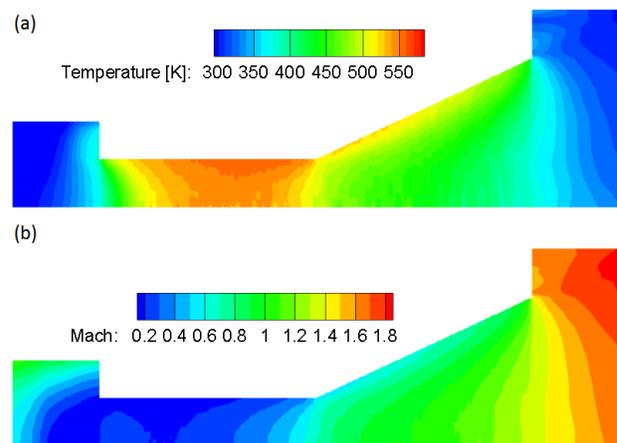
Fig. 13.   Temperature (a) and Mach number (b) maps for the second-half divergent microchannel (case 3), for a divergent angle of 25 degrees, plenum pressure of 150 Pa and wall temperature of 573 K.

on the divergent angle in the second part. The transmission coefficient is never larger than 31% (value for a cylindrical tube with aspect ratio of 2.5), in accordance to the results obtained in [11], and the largest transmission coefficient is achieved for an angle of 25 degrees.

3.5   Case 4. First-half divergent microchannel analysis

Following the analysis of case 3, a conclusion is that when the highest gas temperature (wall temperature) is achieved due to a high number of collisions, the mass flow rate is lower and when the mass flow rate is increased due to the increased divergent angle, the number of collisions decreases and the gas temperature is lower. In order to combine these effects, in case 4 the first half of the microchannel (divergent) is used for the thermal expansion to increase the mass flow rate, and the second half (constant area) is used

Table 7. Knudsen number at the channel inlet and outlet, second-half divergent microchannel (case 3), for different divergent angles at a plenum pressure of 150 Pa and wall temperature of 573 K.

$\beta[°]$	05	10	15	20
Kn_{in}	0.5	0.5	0.5	0.5
Kn_{out}	11.2	16.9	24.6	34.7
$\prod$	25.4	40.4	62.7	95.9
$\beta[°]$	25	30	35	40
Kn_{in}	0.5	0.5	0.5	0.5
Kn_{out}	47.8	64.8	86.4	114.3
$\prod$	144.4	217.0	322.0	479.6
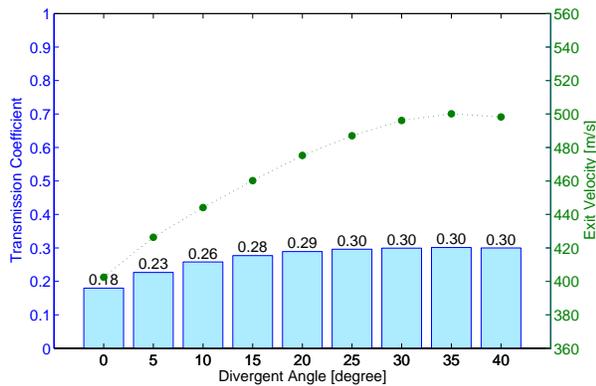
Fig. 14. Transmission coefficient and exit velocity for different divergent angles at a plenum pressure of 150 Pa and wall temperature of 573 K, second- half divergent microchannel (case 3).

Fig. 15. Mean pressure along the channel, first-half divergent microchannel (case 4), for different divergent angles at a plenum pressure of 150 Pa and wall temperature of 573 K.

Fig. 16. Mean temperature along the channel, first-half divergent microchannel (case 4), for different divergent angles at a plenum pressure of 150 Pa and wall temperature of 573 K.

to increase the temperature. Figure 15 shows that the entrance pressure decreases significantly as it happened for the entirely divergent angle (case 2), but presents a smoother increase when compared to case 2. Additionally, the gas temperature through the channel is larger than case 2, compare Figures 8 and 16.

The complete temperature field in the channel can be seen in Figure 17 as well as the Mach number map. In the first half of the microchannel, the Mach number presents a similarity to case 2, reaching a value of 0.6 in the beginning of the channel due to the thermal expansion, while the situation in the second half is similar to case 1 and the Mach number tends again to reach the sonic regime at the end of the microchannel, see the example in Figure 17-(b). In this case the flow goes in the free molecular regime just at the channel exit, for a divergent angle higher than 15 degrees, see Table 8.

The exit velocity does not show a significant change with the divergent angle, and the highest exit velocity (413.3 m/s) is achieved for a divergent angle of 10 degrees, see Figure 18. On the other hand, the transmission coefficient increases significantly with increasing the divergent angle. This result is comparable to the case of entirely divergent
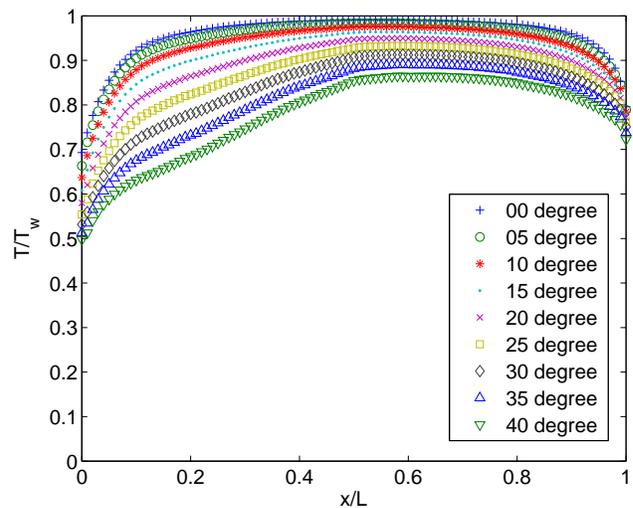
channel (case 2). Another interesting result is that a divergent angle of 40 degrees shows almost the same exit velocity as the baseline, but with a very high transmission coefficient of 91%.

3.6 Thruster performance analysis

Each one of the studied cases shows its own specific flow characteristics, as previously described. In case the microchannels are used as flow acceleration elements in a space thruster, these characteristics can be used to compute the expected propulsion performance (thrust, specific impulse and power consumption, in particular). This subsection will present the propulsion performance and the different parameters that influence it directly.

Figure 19 shows how the exit velocity profile along the
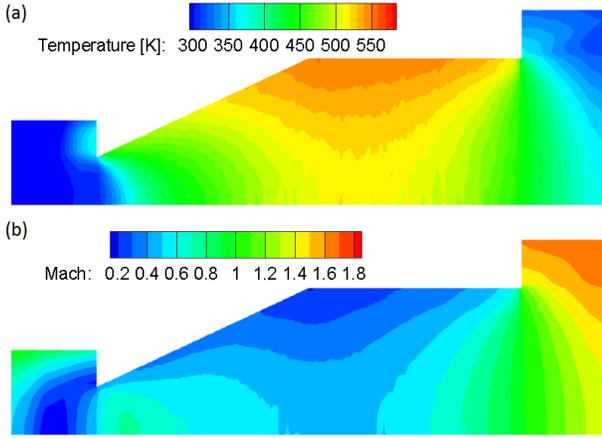
Fig. 17.   Temperature (a) and Mach number (b) maps for the first-half divergent microchannel (case 4), for a divergent angle of 25 degrees, plenum pressure of 150 Pa and wall temperature of 573 K.

Fig. 18.   Transmission coefficient and exit velocity for different divergent angles at a plenum pressure of 150 Pa and wall temperature of 573 K, first-half divergent microchannel (case 4).

Table 8.   Knudsen number at the channel inlet and outlet, first-half divergent microchannel (case 4), for different divergent angles at a plenum pressure of 150 Pa and wall temperature of 573 K.

$\beta[°]$	05	10	15	20
Kn_{in}	0.5	0.5	0.5	0.6
Kn_{out}	7.5	8.5	10.1	12.3
Π	15.1	15.6	16.8	18.5
$\beta[°]$	25	30	35	40
Kn_{in}	0.6	0.6	0.6	0.6
Kn_{out}	15.2	18.9	23.8	30.1
Π	20.9	24.3	28.9	35.1

Fig. 19.   Velocity profile along the y axis at the channel exit (x = 500 μm), for all cases, with a divergent angle of 25°.

y axis is influenced by the channel geometry. In particular, a divergent angle at the channel exit makes the flow significantly more bi-dimensional, with a less uniform axial component of the exit velocity and a non negligible component of it along the y axis. This effect becomes even more prominent at higher divergent angles, as shown in Table 9, where the maximum V_y/V_x ratio at the channel exit (for y/r = 1) is shown for all cases and different values of the divergent angle.

From the baseline (case 1), Figure 20 shows the relationship between thrust and specific impulse under different plenum pressure and channel wall temperature. In Figure 20, lines are drawn for constant wall channel temperature and constant plenum pressure. It shows that the specific impulse increases when the channel wall temperature increases and the thrust increases significantly with the plenum pressure and also, slightly, with the channel wall temperature.

Another important result is obtained in relation to specific energy, that is the ratio of power (thermal energy) consumption per mass flow rate. Figure 21 shows that the specific energy rises with the wall temperature and, consequently, the specific impulse. An increase in plenum pres-

sure tends to slightly decrease the specific energy.

The specific impulse basically increases when the gas temperature increases as a consequence of the higher wall temperature, or when the molecular mass decreases by changing the molecular species, as it is already shown by [9]. On the other hand, the thrust can be increased by increasing the plenum pressure, the channel wall temperature, the exit area or the transmission coefficient, as also shown by [9]. However, the channel wall temperature does not affect significantly the thrust and is obviously also limited by the material properties. For what concerns the plenum pressure, when it is increased the flow tends to move from the rarefied gas regime to the continuum flow one, for which completely different equations and considerations should be applied. It is obviously also possible to increase the flow exit area by increasing the number of slots/microchannels, at least up to a certain level after which a too large heater chip and plenum volume would be obtained. The transmission coefficient depends basically on the geometry and, in particular, the aspect

Table 9. Maximum V_y/V_x ratio at the channel exit (for y/r = 1), for all cases and different values of the divergent angle.

	$\left(\dfrac{V_y}{V_x}\right)_{max}$	Case 2	Case 3	Case 4
	0°	0.2035	0.2035	0.2035
	5°	0.2400	0.2399	0.2169
	10°	0.2808	0.2823	0.2148
	15°	0.3253	0.3227	0.2225
β	20°	0.3752	0.3810	0.2132
	25°	0.4364	0.4371	0.2160
	30°	0.5089	0.5166	0.2178
	35°	0.5936	0.6029	0.2174
	40°	0.6943	0.6943	0.2222

Fig. 21. Specific energy versus specific impulse for different values of the plenum pressure and wall temperature, baseline microchannel (case 1).

Fig. 20. Thrust versus specific impulse for different values of the plenum pressure and wall temperature, baseline microchannel (case1).

Fig. 22. Thrust and specific impulse as functions of the divergent angle, for plenum pressure of 150 Pa and wall temperature of 573 K (cases 2, 3 and 4).

ratio. However, when the aspect ratio decreases, the heat transfer becomes less effective and thus the gas temperature and specific impulse decrease. The power consumption is crucial, since it is one of the most important design drivers of satellites, especially small ones, with limited power available. In summary, it is desirable to achieve the maximum possible thrust and specific impulse with the minimum power consumption.

Figure 22 shows a comparison among different geometries, at plenum pressure of 150 Pa and channel wall temperature of 573 K. For the entirely divergent channel, case 2, when the angle increases the thrust increases dramatically due to the increased transmission coefficient, and the specific impulse decreases significantly due to the lower gas temperature. For the second-half divergent angle, case 3, the aspect ratio of the first part of the microchannel represents a sort of "barrier" to the mass flow rate, so the thrust does not change much and the specific impulse decreases significantly with the angle. For the first-half divergent angle, case 4, the thrust increases significantly with the angle in the same way as case 2, and the specific impulse slightly decreases.

As it can be seen in Figure 23 the specific energy presents an interesting behaviour. In case 3 there is a slight decrease of specific energy with a divergent angle up to 10 degrees, followed by a significant increase for higher divergent angles. In cases 2 and 4 there is a significant decrease in the specific energy with the divergent angle.

In space propulsion, the total thrust produced by a system is generated by two different contributions: the momentum thrust (caused by change of momentum in the fluid) and the pressure thrust (caused by pressure difference between channel exit and ambient), see Equation 2. Each contribution plays a different role for different cases. In the baseline case, case 1, the pressure thrust represents 42 % of the total thrust. In cases 2 and 3, where the exit pressure decreases due to the divergent angle, the pressure thrust becomes a smaller portion of the total thrust, just 19 % for a divergent angle of 40 degrees. In case 4, with the same divergent angle, the pressure thrust represents again a larger portion of the total thrust (about 40 %), due to the heat transfer in the second half of the microchannel. In any case, it is clear that the pressure thrust contribution is not negligible in this concept, differently to
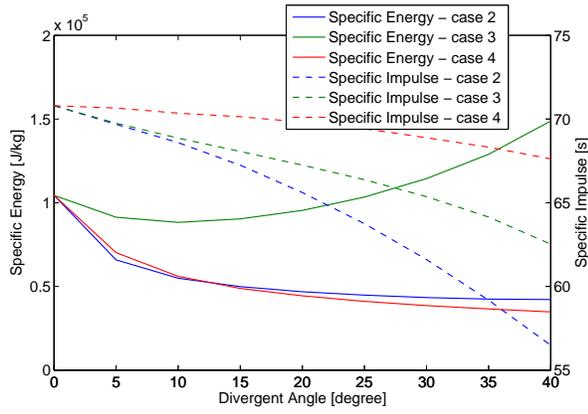
Fig. 23. Specific energy and specific impulse as functions of the divergent angle, for plenum pressure of 150 Pa and wall temperature of 573 K (cases 2, 3 and 4).

what happens in more traditional propulsion systems especially then used under vaccum conditions.

4 Conclusion

The DSMC method was applied to simulate the flow and thermal behaviour in four different microchannels geometries for a FMMR devices. The baseline case with constant channel area was analysed to study the influence of different plenum pressures and channel wall temperatures on the mass flow rate, thrust and specific impulse. The other cases, in which a divergent section is presented in the channel, a plenum pressure of 150 Pa and channel wall temperature of 573 K have been considered, but a divergent angle range from 0 to 40 degrees was used with different configurations (entirely divergent, only first half or only second half). In addition, the heat transfer and fluid flow in the microchannels has been discussed.

It is shown that the transmission coefficient increases significantly with increasing divergent angle, which improves the mass flow rate through the channel and, consequently, the thrust. On the other hand, when the divergent angle increases, the heat transfer effectiveness tends to decrease significantly, which influences in a negative way the exit velocity. It has been shown that the case of first-half divergent channel is the best combination of these two contrasting effects. In terms of thrust performance, therefore, this is the most promising case. It combines a relatively small reduction of specific impulse with a significant increase of thrust. As a comparison, the thrust of one microchannel with divergent angle of 40 degrees in this case is equivalent to 4.8 microchannels of the baseline case, with a specific impulse decrease of just 5% and a reduction in power consumption of 66.7%, considering a plenum pressure of 150Pa and a channel wall temperature of 573K.

In order to use these findings in an actual propulsion system design, further investigations need to be carried out. A propellant needs to be selected that can be stored easily in a small volume with low mass, allowing to design a sim-

ple final product with low number of components and, at the same time, keep an adequate thrust performance. A characterization of the heater chip in a test environment and a flight validation on a nano- or pico-satellite mission will be very important to this respect.

Nomenclature

A_e Thruster exit area [m^2]
b Constant dependent on the derivatives of velocity profile
B Constant dependent on $\tilde{P} = P(x = 0)/P_o$
c Speed of sound [m/s]
$\bar{c} = \sqrt{8kT/\pi m}$ Mean thermal speed [m/s]
d_{ref} Reference molecular diameter [m]
g_0 Earth gravitational acceleration at sea level [m/s^2]
I_{sp} Specific Impulse [s]
k Boltzmann constant [J/kg]
Kn Knudsen number [dimensionless]
Kn_{in} Inlet Knudsen number [dimensionless]
Kn_{out} Outlet Knudsen number [dimensionless]
L_0 Characteristic dimension [m]
L Length of the channel [m]
m Molecular mass [kg]
$\dot{m}$ Mass flow rate [kg/s]
$\dot{m}_{fm}$ Mass flow rate in the free molecular limit [kg/s]
M_a Mach number [dimensionless]
P_a Ambient pressure [Pa]
P_e Pressure at the nozzle exit [Pa]
P_0 Plenum pressure [Pa]
$\tilde{P}$ Ratio of local pressure to outlet pressure [dimensionless]
r Microchannel radius [m]
T Temperature [K]
T_0 Plenum temperature [K]
T_w Channel wall temperature [K]
u_e Exit velocity [m/s]
V_x Velocity along the x axis [m/s]
V_y Velocity along the y axis [m/s]
α Transmission coefficient
$\bar{\alpha}$ parameter which depends on Kn
β Divergence angle [degree]
Δx_{cell} Cell size [m]
Δt_{step} Time step [s]
λ Mean free path [m]
ξ Fraction of mean free time (the mean time between collisions) at the mean stream conditions [dimensionless]
$\prod$ Ratio of channel's inlet pressure to channel's outlet pressure [dimensionless]

σ_v Thermal accommodation [dimensionless]

ω Temperature coefficient of viscosity [dimensionless]

$\Im$ Thrust [N]

References

[1] B. Sanders, L. Van Vliet, F. Tata Nardini, T. Gronland, P. Rangsten, H. Shea, M. Noca, R. Visee, B. Monna, J. Stark, A. Bulit, D. M. Di Cara, 2010. "Development of MEMS based Electric Propulsion". 3AF, ESA and CNES, Space Propulsion Conference 2010.

[2] J. Guo, J. Bouwmeester, E. Gill, 2014. "In-Orbit Results of Delfi-N3xt: Lessons Learned and Move Forward". International Astronautical Federation, 65th International Astronautical Congress.

[3] A. Cervone, B. Zandbergen, J. Guo, E. Gill, W. Wieling, F. Tata Nardini, C. Schuurbiers, 2012. "Application of an Advanced Micro-Propulsion System to the DELFFI Formation-Flying Demonstration within the QB50 Mission". International Astronautical Federation, 63rd International Astronautical Congress.

[4] E. Gill, P. Sundaramoorthy, J. Bouwmeester, B. Zandbergen, R. Reinhard, 2013. "Formation flying within a constellation of nano-satellites: The qb50 mission". *Acta Astronautica,* **82**, pp. 110–117.

[5] A. S. Gohardani, J. Stanojev, A. Demaire, K. Anflo, M. Persson, N. Wingborg, C. Nilsson, 2014. "Green space: Opportunities and propects". *Progress in Aerospace Sciences,* **71**, pp. 128–149.

[6] A. Ketsdever, D. Wadsworth, S. Vargo, E. Muntz, 1998. "A free Molecule Micro-Resistojet: An Interesting Alternative to Nozzle Expansion". AIAA/ASME/SAE/ASEE, 34th AIAA/ASME/SAE/ASEE Joint Propulsion Conference and Exhibit.

[7] A. Cervone, A. Mancas, B. Zandbergen, 2015. "Conceptual design of a low-pressure micro-resistojet based on a sublimating solid propellant". *Acta Astronautica,* **108**, pp. 30–39.

[8] D. C. Guerrieri, M. de Athayde Costa e Silva, B. T. C. Zandbergen, A. Cervone, 2015. "Development of a Low Pressure Free Molecular Micro-Resistojet for CubeSat Applications". International Astronautical Federation, 66th International Astronautical Congress.

[9] A. Ketsdever, R. Lee, T. Lilly, 2005. "Performance testing of a microfabricated propulsion system for nanosatellite applications". *Journal of Micromechanics and Microengineering,* **15**, pp. 2254–2263.

[10] Z. Ahmed, S. F. Gimelshein, A. Ketsdever, 2005. "Numerical Analysis of Free Molecule Micro-Resistojet Performance". AIAA/ASME/SAE/ASEE, 41st AIAA/ASME/SAE/ASEE Joint Propulsion Conference and Exhibit.

[11] J. M. Lafferty, 1998. *Foundations of Vaccum Science and Technology*. John Wiley and Sons.

[12] E. P. Muntz, 1989. "Rarefied gas dynamics". *Annual Review of Fluid Mechanics,* **21**, pp. 387–422.

[13] B. D. Tuckerman, R. F. W. Pease, 1981. "High-performance heat sinking for vlsi". *Electron Device Letters, IEEE,* **2**, pp. 126–129.

[14] G. Karniadakis, A. Beskok, N. Aluru, 2005. *Microflows and Nanoflows Fundamentals and Simulation*, Vol. 29 of *0939-6047*. Springer-Verlag New York.

[15] G. A. Bird, 1994. *Molecular Gas Dynamics and the Direct Simulation of Gas Flow*. Oxford Engineering Science Series (Book 42). Clarendon Press.

[16] W. Wagner, 1992. "A convergence proof for bird's direct simulation monte carlo method for the boltzmann equation". *Journal of Statistical Physics,* **66**, pp. 1011–1044.

[17] H. Akhlaghi, M. Balaj, E. Roohi, 2013. "Direct simulation monte carlo invertigation of mixed supersonic-subsonic flow through micro-/nano-scale channels". *Physica Scripta,* **88**, p. 015401.

[18] C. Mavriplis, J. C. Ahn, R. Goulard, 1997. "Heat transfer and flowfields in short microchannels using direct simulation monte carlo". *Journal of Thermophysics and Heat Transfer,* **11**(4), pp. 489–496.

[19] M. Balaj, E. Roohi, H. Akhlaghi, R. S. Myong, 2014. "Investigation of convective heat transfer through constant wall heat flux micro/nano channel using dsmc". *International Journal of Heat and Mass Transfer,* **71**, pp. 633–638.

[20] S. Varoutis, D. Valougeorgis, O. Sazhin, F. Sharipov, 2008. "Rarefied gas flow through short tubes into vaccum". *Journal Vacuum Science Technology,* **26**, p. 228.

[21] Seyed Ali Saadati, Ehsan Roohi, 2015. "Detailed investigation of flow and thermal field in micro/nano nozzles using simplified bernoulli trial (sbt) collision scheme in {DSMC}". *Aerospace Science and Technology,* **46**, pp. 236–255.

[22] M. R. Wang, Z. X. Li, 2004. "Numerical simulations on performance of mems-based nozzles at moderate or low temperatures". *Microfluidics and Nanofluidics,* **1**, pp. 62–70.

[23] H. Horisawa, F. Sawada, K. Onodera, I. Funaki, 2008. "Numerical simulation of micro-nozzle and micro-nozzle-array flowfield characteristics". *Vacuum,* **83**, pp. 52–56.

[24] M. S. Ivanov, G. N. Markelov, A. D. Ketsdever, D. C. Wadsworth, 1999. "Numerical Study of Cold Gas Micronozzle Flows". AIAA 99-0166, 37th Aerospace Sciences Meeting and Exhibit.

[25] Oleg Sazhin, 2008. "Dsmc-computation of the rarefied gas flow through a slit into a vacuum". *Journal Vacuum Science Technology,* **1084**, pp. 1147–1152.

[26] E.S. Oran, C.K. Oh, B.Z. Cybyk, 1998. "Direct simulation monte carlo: Recent advances and applications". *Annual Review of Fluid Mechanics,* **30**(1), pp. 403–441.

[27] T. J. Scanlon, E. Roohi, C. White, M. Darbandi, J. M. Reese, 2010. "An open source, parallel dsmc code for rarefied gas flows in arbitrary geometries". *Computers and Fluids,* **39**, pp. 2078–2089.